Phase Retrieval of a Point Spread Function

Nicholas Chimitt[a], Ali Almuallem[a], and Stanley H. Chan[a]

[a]Purdue University, 465 Northwestern Ave, West Lafayette, USA

ABSTRACT

The estimation of a phase aberration by observing a point spread function (PSF), known as wavefront estimation, is a critical problem in adaptive optics. Analogous to phase retrieval, wavefront estimation suffers from multiple ambiguous solutions. Many prior works require multiple structured measurements to overcome this fundamental challenge. In this paper, we use an asymmetric pupil to make what would otherwise be an impossible inverse problem to be possible. We combine this with an efficient machine learning algorithm to overcome remaining non-convexity. We empirically observe asymmetric pupils tend to outperform symmetric pupils.

Keywords: Wavefront estimation, phase retrieval, adaptive optics, computational imaging, machine learning

1. INTRODUCTION

The performance of an optical imaging system is upper limited by diffraction. However, the diffraction limit is often not precisely reached due to limitations imposed by the environment or camera optics.[1] Correcting for these aberrations through adaptive optics boosts the performance of the imaging system by bringing them closer to the diffraction limit. Estimating this aberration well is a critical problem in fields such as astronomy, as well as a long-standing open research problem closely associated with phase retrieval.

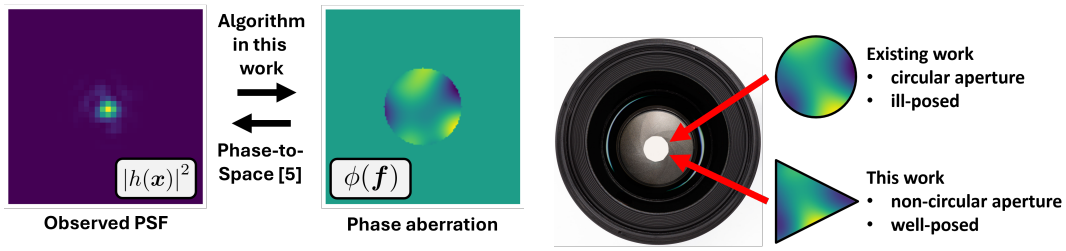

(a) Goal of this work. (b) Using an asymmetric pupil.

Figure 1. (a) The goal of this work is to estimate a phase aberration from a single PSF. (b) A triangular pupil allows one to eliminate origin-centric symmetries inherent to a circular boundary, creating a well-posed inverse problem.

We present a visual representation of the goal of this work in Figure 1(a): given a single measurement of a point spread function (PSF), estimate its phase aberration. Defining a PSF to be,[2]

$$|h(\boldsymbol{x})|^2 = \left|\mathcal{F}\left\{P(\boldsymbol{f})e^{-j\phi(\boldsymbol{f})}\right\}\right|^2, \tag{1}$$

$$\stackrel{\text{def}}{=} \text{PSF}(P,\phi), \tag{2}$$

with $P(\boldsymbol{f})$ as the pupil function and $\phi(\boldsymbol{f})$ as the phase aberration, wavefront estimation can be defined as

$$\phi(\boldsymbol{f}) = \underset{\phi'}{\text{argmin}} \left\| |h(\boldsymbol{x})|^2 - \text{PSF}(P,\phi') \right\|^2. \tag{3}$$

This paper focuses on the use of asymmetric pupils, as highlighted in Figure 1(b), to enable computational recovery of ϕ from $\text{PSF}(P,\phi)$. Introducing an asymmetric pupil to break the symmetries in wavefront retrieval

Further author information: (Send correspondence to N.C.)
N.C.: E-mail: nchimitt@purdue.edu

Unconventional Imaging, Sensing, and Adaptive Optics 2024, edited by Jean J. Dolne, Santasri R. Bose-Pillai, Matthew Kalensky, Proc. of SPIE Vol. 13149, 131491H
 · 0277-786X · doi: 10.1117/12.3028192

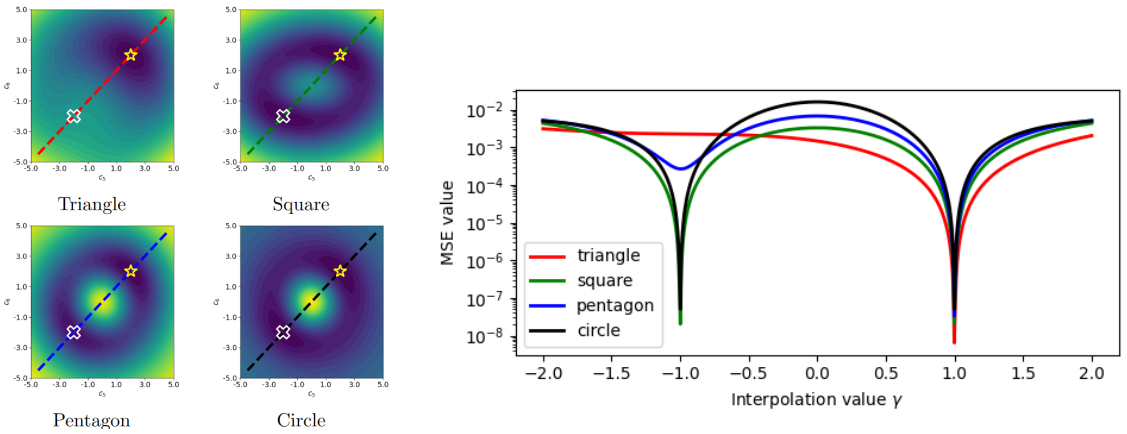

(a) 2D Error (b) Along $c_5 = c_6$.

Figure 2. (a) The optimization landscape of each corresponding $P_k(\boldsymbol{f})$ for the sum of vertical and horizontal astigmatism. We show the loss manifold indicated by yellow for a high value and dark blue for a low value. The line $c_5 = c_6$ is shown as a colored dashed line with $c_5 = c_6 = 2$ indicated by a yellow star and $c_5 = c_6 = -2$ by a white $\times$. (b) The cross-section of the optimization landscape with the colors selected correspondingly.

is not enough to completely solve the problem, although it makes an otherwise highly ill-posed problem possible. To this end, we approximate $\text{PSF}(P, \phi)$ by a learned network[3] and use multiple random initializations.

Two common approaches for directly solving (3) are the Gerchberg-Saxton (GS)[4] and Hybrid Input-Output (HIO)[5] algorithms. These algorithms consist of iterative projections via Fourier transform pairs $\mathcal{F}\{\cdot\}$ and $\mathcal{F}^{-1}\{\cdot\}$ which terminate when both $f(\boldsymbol{x})$ and $\mathcal{F}\{f(\boldsymbol{x})\} = F(\boldsymbol{f})$ satisfy basic constraints. However, there exists solutions for which the corresponding intensity is identical[6] which can be resolved with additional problem-specific constraints[7–11] such as multiple observations,[12–15] often with random codes,[16] or phase diversity.[17] It has also been observed asymmetry in the support tends to help phase retrieval and wavefront estimation.[18–20]

Another way of approaching (3) is by a model on the phase. One such approach is from Fienup using the Zernike polynomials[9] to expand $\phi(\boldsymbol{f}) = \sum_{m=1}^{M} \alpha_m Z_m(\boldsymbol{f})$, with $Z_m(\boldsymbol{f})$ as the Zernike polynomials with Noll's indexing.[21] Defining $\boldsymbol{\alpha} = [\alpha_1, \alpha_2, \ldots, \alpha_M]^T$,[9] (3) can be formulated in terms of $\boldsymbol{\alpha}$. Even though the dimensionality is lower, non-convexity is still present as $\boldsymbol{\alpha}$ is not unique in general . For example, Siddik et al.[22] notes the signs of even Zernike polynomials are the cause of ambiguity in $\boldsymbol{\alpha}$.

2. METHODS

2.1 Toy example: vertical & horizontal astigmatisms

Consider the wavefront estimation problem for a sum of two astigmatisms, vertical and horizontal, which can be modeled as a sum of two Zernike polynomials: $\phi(\boldsymbol{f}) = a_5 Z_5(\boldsymbol{f}) + a_6 Z_6(\boldsymbol{f})$. Here we set $a_5 = a_6 = 2$, with our goal being to estimate $[a_5, a_6]^T$. In Figure 2(a) we present the optimization landscape obtained by probing the set of solutions via $[c_5, c_6]^T$, with the error computed as:

$$\text{Error} = \|\text{PSF}(P_k, \phi) - \text{PSF}(P_k, c_5 Z_5(\boldsymbol{f}) + c_6 Z_6(\boldsymbol{f})\|^2. \tag{4}$$

We expect the error to be minimized when $c_5 = c_6 = 2$ which we indicate with a star in Figure 2 and the incorrect "twin" solution at $c_5 = c_6 = -2$ with a white $\times$. We also evaluate the loss along $c_5 = c_6$ in Figure 2(b). We define γ to be $[c_5, c_6]^T = \gamma \odot [a_5, a_6]^T$. One can observe that the triangle and pentagon have unique global minima along $c_5 = c_6$ while the square and circle have two global minima along $c_5 = c_6$.

2.2 Approximating the wavefront estimation problem

Although asymmetry has some impact to the problem's behavior, it still remains largely non-convex. One possibility is to use multiple random initialiations,[23] though solving (3) in such a way will produce a significant

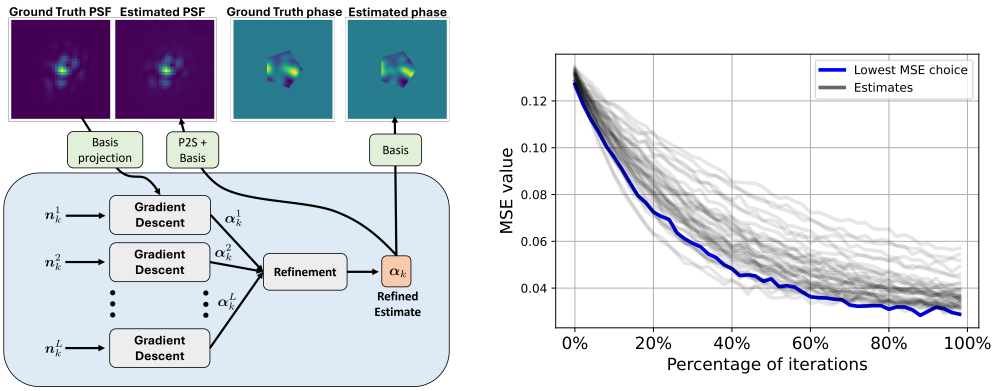

(a) Algorithm (3) overview (b) MSE trajectory

Figure 3. (a) Overview of algorithm (3). A PSF is decomposed and given as input to the algorithm which solves for multiple estimates in parallel given different initializations. (b) Illustration of the MSE refinement. Given different starting points, estimates may converge to different estimates with trajectories shown in semi-transparent black with the lowest MSE error at the final iteration highlighted in blue.

computational burden, requiring thousands of Fourier transforms iterativey. This motivates us to approximate the wavefront estimation problem (3) using the Phase-to-Space (P2S) transform from Mao et al.[3] Following Mao et al., we expand ϕ and the PSF via basis functions:

$$P_k(\boldsymbol{f}) \odot \phi(\boldsymbol{f}) \approx \sum_{m=1}^{M} \alpha_{k,m}\zeta_{k,m}(\boldsymbol{f}) \tag{5}$$

$$\text{PSF}\,(P_k, \phi) \approx \sum_{n=1}^{N} \beta_{k,n}\varphi_{k,n}(\boldsymbol{x}). \tag{6}$$

To obtain orthogonal $\zeta_{k,m}$ over polygons, we use a finite element solver[24] to solve for the eigenfunctions of the Poisson equation over k-sided polygon and refer to the eigenfunctions as $\zeta_{k,m}$. The basis functions $\varphi_{k,n}$ are obtained by principal component analysis (PCA) on a dataset of PSFs.

Defining $\boldsymbol{\alpha} = [\alpha_1, \alpha_2, \ldots, \alpha_M]^T$ and $\boldsymbol{\beta} = [\beta_1, \beta_2, \ldots, \beta_M]^T$, the P2S is a learned mapping to approximate

$$\underbrace{\text{P2S}(P_k, \boldsymbol{\alpha}_k)}_{\text{neural network}} \approx \boldsymbol{\beta}_k. \tag{7}$$

We use the P2S operator to replace the PSF operator, leading to:

$$\boldsymbol{\alpha}_k \approx \underset{\boldsymbol{\alpha}'_k}{\text{argmin}} \left\|\boldsymbol{\beta}_k - \text{P2S}(P_k, \boldsymbol{\alpha}'_k)\right\|^2. \tag{8}$$

We solve (8) through gradient descent. Although (8) is computationally efficient, there still exists non-convexity. We propose to use this efficiency to solve (8) through gradient descent with L random initializations $\{\boldsymbol{n}_k^\ell\}_{\ell=1}^L$, where $\boldsymbol{n}_k^\ell$ is a zero-mean Gaussian vector. This produces a population of estimates which we then select the solution which minimizes the MSE of (8) which we refer to MSE refinement. The algorithm is shown in Figure 3(a). In Figure 3(b) we present an illustration of the MSE for the population of estimates at each iteration.

3. EXPERIMENTS

3.1 Data generation and P2S training

We generate Gaussian random fields with squared exponential covariance for $\phi_t(\boldsymbol{f})$ using fast Fourier transform (FFT) based sampling methods.[25] We then window them by $P_k(\boldsymbol{f})$ and generate corresponding PSFs. Each $P_k(\boldsymbol{f})$ is generated in such a way that their areas are consistent. We additionally remove the DC shift term and

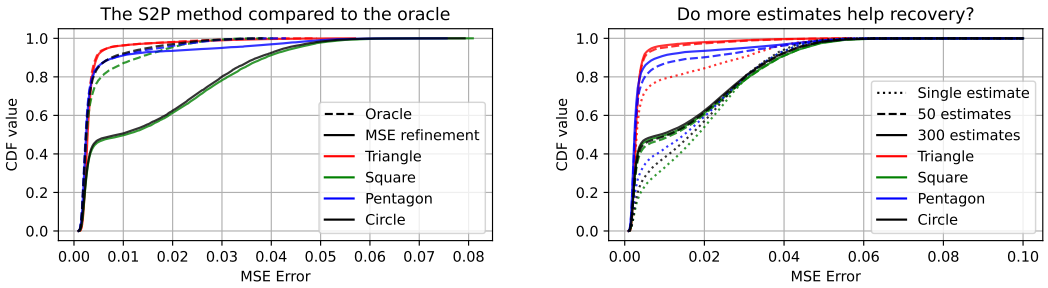

(a) CDF of algorithm vs. oracle (b) Impact of multiple estimates

Figure 4. (a) The CDF of the MSE refinement compared to the CDF of the oracle estimator. Solid lines correspond to the MSE refinement and dashed lines correspond to the oracle. (b) The CDF of the MSE error for different amounts of parallel estimates and pupil shapes.

"tilt" term from each generated $P_k(\boldsymbol{f}) \odot \phi_t(\boldsymbol{f})$. Our dataset then comes from the corresponding decompositions (5) and (6). We train a P2S transform per pupil $P_k(\boldsymbol{f})$ to approximate the loss (7) in a MSE sense using 50,000 training samples. Our testing data comes from the same distribution as training data.

3.2 Performance of proposed algorithm

Suppose the final refined estimate of the algorithm is $\boldsymbol{\alpha}_k$. Introducing $\boldsymbol{\phi}$, $\boldsymbol{P}_k$, and $\boldsymbol{\zeta}_{k,m}$ as the discretized form of their respective continuous functions, we can define the error as a random variable

$$X = \frac{\left\| \boldsymbol{\phi} - \sum_{m=1}^{M} \alpha_{k,m} \boldsymbol{\zeta}_{k,m} \right\|^2}{\|\boldsymbol{P}_k\|}. \tag{9}$$

We analyze the cumulative distribution function (CDF), i.e., $F_X(x) = \mathbb{P}[X \leq x]$ for the different polygon pupils using (8). We also measure the performance of the following "oracle" according to (9). Given a set of estimates $\{\boldsymbol{\alpha}_k^\ell\}_{\ell=1}^L$, we define the oracle to be

$$\ell^* = \underset{\ell}{\operatorname{argmin}} \left\| \boldsymbol{\phi} - \sum_{m=1}^{M} \alpha_{k,m}^\ell \boldsymbol{\zeta}_{k,m} \right\|^2. \tag{10}$$

In Figure 4(a) we compare the oracle to MSE refinement with 300 estimates. While asymmetric polygons perform closely to their oracle counterpart, symmetric polygons tend to leave a wide gap in performance. Figure 4(b) shows the impact that using parallel estimates. We can see that the circle, square, and even the pentagon perform poorly for a single estimate. However, upon using multiple estimates, the pentagon improves dramatically whereas the circle and square improve marginally. Note that this should not be confused with the concept of multiple *measurements*; there is only one available measurement which we are solving by multiple initializations.

4. CONCLUSION

In this paper, we described using a learned transform and multiple random initializations to overcome non-convexity for recovering the phase aberration from a single PSF. Empirically we observe that asymmetric pupils tend to outperform symmetric pupils in the noiseless case. Furthermore, we observe that using multiple random initializations helps to overcome the remaining non-convexity. Future work will be aimed at understanding optimal pupil geometry and studying performance in noise.

ACKNOWLEDGMENTS

This material is based upon work supported by the National Science Foundation under Grant No. 2133032, 2030570, 2134209. Any opinions, findings, and conclusions or recommendations expressed in this material are those of the author(s) and do not necessarily reflect the views of the National Science Foundation.

REFERENCES

[1] Chan, S. H. and Chimitt, N., "Computational imaging through atmospheric turbulence," *Foundations and Trends® in Computer Graphics and Vision* **15**(4), 253–508 (2023).

[2] Goodman, J. W., [*Introduction to Fourier optics*], Roberts and Company publishers (2005).

[3] Mao, Z., Chimitt, N., and Chan, S. H., "Accelerating atmospheric turbulence simulation via learned Phase-to-Space transform," (2021).

[4] Gerchberg, R. W.; Saxton, W. O., "A practical algorithm for the determination of the phase from image and diffraction plane pictures," *Optik* (35), 237—246 (1972).

[5] Fienup, J. R., "Phase retrieval algorithms: a comparison," *Applied optics* **21**(15), 2758–2769 (1982).

[6] Ranieri, J., Chebira, A., Lu, Y. M., and Vetterli, M., "Phase retrieval for sparse signals: Uniqueness conditions," *arXiv preprint arXiv:1308.3058* (2013).

[7] Fienup, J. R. and Wackerman, C., "Phase-retrieval stagnation problems and solutions," *JOSA A* **3**(11), 1897–1907 (1986).

[8] Seldin, J. and Fienup, J., "Numerical investigation of the uniqueness of phase retrieval," *JOSA A* **7**(3), 412–427 (1990).

[9] Fienup, J. R., "Phase-retrieval algorithms for a complicated optical system," *Applied optics* **32**(10), 1737–1746 (1993).

[10] Fienup, J. R., Marron, J. C., Schulz, T. J., and Seldin, J. H., "Hubble space telescope characterized by using phase-retrieval algorithms," *Appl. Opt.* **32**, 1747–1767 (Apr 1993).

[11] Tian, Y. and Fienup, J. R., "Phase retrieval with only a nonnegativity constraint," *Optics Letters* **48**(1), 135–138 (2023).

[12] Misell, D., "A method for the solution of the phase problem in electron microscopy," *Journal of Physics D: Applied Physics* **6**(1), L6 (1973).

[13] Rodenburg, J. M., "Ptychography and related diffractive imaging methods," *Advances in imaging and electron physics* **150**, 87–184 (2008).

[14] Candès, E. J., Strohmer, T., and Voroninski, V., "PhaseLift: Exact and stable signal recovery from magnitude measurements via convex programming," *Communications on Pure and Applied Mathematics* **66**(8), 1241–1274 (2013).

[15] Möckl, L., Petrov, P. N., and Moerner, W. E., "Accurate phase retrieval of complex 3D point spread functions with deep residual neural networks," *Applied Physics Letters* **115**, 251106 (12 2019).

[16] Candès, E. J., Li, X., and Soltanolkotabi, M., "Phase retrieval from coded diffraction patterns," *Applied and Computational Harmonic Analysis* **39**(2), 277–299 (2015).

[17] Feng, B. Y., Guo, H., Xie, M., Boominathan, V., Sharma, M. K., Veeraraghavan, A., and Metzler, C. A., "NeuWS: Neural wavefront shaping for guidestar-free imaging through static and dynamic scattering media," *Science Advances* **9**(26), eadg4671 (2023).

[18] Cederquist, J. N., Fienup, J. R., Wackerman, C. C., Robinson, S. R., and Kryskowski, D., "Wave-front phase estimation from fourier intensity measurements," *J. Opt. Soc. Am. A* **6**, 1020–1026 (Jul 1989).

[19] Martinache, F., "The asymmetric pupil fourier wavefront sensor," *Publications of the Astronomical Society of the Pacific* **125**(926), 422 (2013).

[20] Bos, S. P., Doelman, D. S., Lozi, J., Guyon, O., Keller, C. U., Miller, K. L., Jovanovic, N., Martinache, F., and Snik, F., "Focal-plane wavefront sensing with the vector-apodizing phase plate," *A&A* **632**, A48 (2019).

[21] Noll, R. J., "Zernike polynomials and atmospheric turbulence," *JOSA* **66**(3), 207–211 (1976).

[22] Siddik, A. B., Sandoval, S., Voelz, D., Boucheron, L. E., and Varela, L., "Deep learning estimation of modified zernike coefficients and recovery of point spread functions in turbulence," *Optics Express* **31**(14), 22903–22913 (2023).

[23] Weller, D. S., Pnueli, A., Divon, G., Radzyner, O., Eldar, Y. C., and Fessler, J. A., "Undersampled phase retrieval with outliers," *IEEE Transactions on Computational Imaging* **1**(4), 247–258 (2015).

[24] Gustafsson, T. and McBain, G. D., "scikit-fem: A Python package for finite element assembly," *Journal of Open Source Software* **5**(52), 2369 (2020).

[25] Schmidt, J. D., [*Numerical simulation of optical wave propagation with examples in MATLAB*], SPIE Bellingham, WA, Bellingham, WA (2010).